

Vector Control of Magnetically Modulated Motor for Power Splitting of HEV Application

Toshihiko Noguchi^{1*}, Sawanth Krishna Machavolu¹, Masahiro Aoyama¹ and Yuto Motohashi¹
¹ Graduate School of Integrated Science and Technology, Shizuoka University, Hamamatsu, Japan
 *E-mail: noguchi.toshihiko@shizuoka.ac.jp

Abstract— This paper describes a vector control method of a magnetically modulated motor. The motor has a quite different structure from a standard permanent magnet synchronous motor (PMSM) because of the two rotors with two different mechanical output shafts, i.e., an inner PM rotor and an outer magnetic-flux modulator composed of only iron and air. Investigation on the vector control method using a real machine is still unexplored, thus, the paper discusses the vector control algorithm of the motor. In addition, several experimental tests have been conducted to examine the control performance of the mechanical output power delivered by the two rotors, using a prototype machine. It has been verified that the discussed algorithm makes it possible to control the two rotor output power as well as the stator input power like a conventional planetary-gear-based HEV system, including the motoring and regenerating operations.

Keywords— Hybrid vehicle, magnetically modulated motor, power split, vector control.

I. INTRODUCTION

In order to enhance integration of a hybrid electric vehicle (HEV) power train with a power split mechanism, a magnetically modulated motor (MMM) is supposed to be one of the solutions and has been studied intensively in recent years. There are two rotors in the MMM, i.e., an inner rotor with permanent magnets (PMs) and an outer rotor which works as a magnetic flux modulator [1], [2]. The mechanical power is basically transferred to the drive shaft by the outer rotor, and the mechanical engine power is provided through the inner rotor in a standard application. The electric power is supplied to the stator by the external power converter such as an inverter, and is converted to the mechanical power like a conventional motor. The MMM is possible to synthesize the mechanical engine power and the electrical motor power given by an inverter through the stator, and is capable to deliver the synthesized mechanical power to the drive shaft through the modulator. In addition, it is possible to regenerate the surplus mechanical power from the engine to the inverter if the drive shaft does not require higher power than the engine output. The outer rotor modulates the stator rotating magnetic flux, and the inner PM rotor receives the modulated magnetic flux to generate the electromagnetic torque. Various high-frequency components are generated through the magnetic flux modulation process, which do not contribute to generate

the effective mechanical power. These extra harmonic components of the magnetic flux cause additional power losses, e.g., an eddy current loss in the PM and extra iron losses in the rotor [3]. Therefore, optimization of the motor geometry is significantly important to reduce the power losses in the MMM, where an FEM based electromagnetic analysis plays an important role for the optimization [4]. However, technical discussion on the control scheme of the MMM looks relatively inactivated by researchers in the motor drive field, probably due to its electrical and mechanical complexity [5].

The voltage equation of the MMM have been investigated because the mathematical motor model is the basis of the vector control algorithm. The voltage equation has been derived from a simplified magnetic circuit of the MMM [6]. In this paper, this fundamental investigation is described, and the operation principle is verified with a prototype of the MMM.

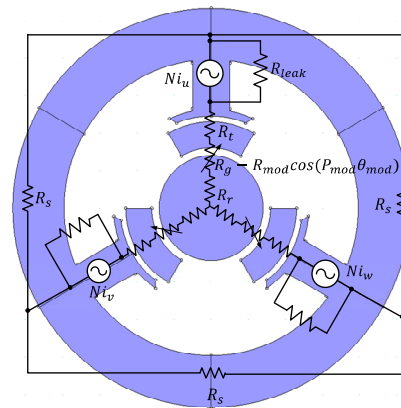


Fig. 1. Simplified MMM model and magnetic circuit.

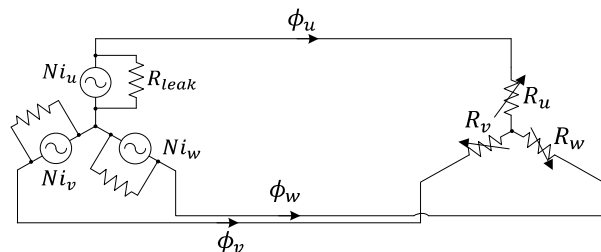


Fig. 2. Three-phase magnetic circuit of MMM.

II. DERIVATION OF VOLTAGE EQUATION

It is assumed that the MMM discussed in the paper has $P_s : P_{pm} : P_{mod} = n : 2n : 3n$ (n is a positive integer) relationship, where P_s is the pole pair number of the stator, P_{pm} is the pole pair number of the inner PM rotor, and P_{mod} is the number of the modulator iron cores. Fig. 1 shows the most fundamental geometry and its magnetic circuit of the MMM, where the least combination of $P_s : P_{pm} : P_{mod} = 1 : 2 : 3$ ($n = 1$) is assumed. Although the MMM is a kind of synchronous machines, it has different pole pair numbers between the stator and the rotor. In the magnetic circuit, the following reluctances are considered; the stator back yoke reluctance \mathcal{R}_b , the stator tooth reluctance \mathcal{R}_t , the air gap reluctance \mathcal{R}_g , the modulator reluctance \mathcal{R}_{mod} , the inner PM rotor core reluctance \mathcal{R}_r , and the reluctance corresponding to the total leakage flux \mathcal{R}_{leak} . N is the number of the winding turns for each phase.

The total reluctance of the three phases \mathcal{R}_u , \mathcal{R}_v , and \mathcal{R}_w are expressed by the following equation because the three-phase reluctance variations caused by the modulator are in phase with each other:

$$\begin{aligned} \mathcal{R}_u &= \mathcal{R}_v = \mathcal{R}_w = \mathcal{R}_{dc} - \mathcal{R}_{mod} \cos(P_{mod} \theta_{mod}) \\ \therefore \mathcal{R}_{dc} &= \mathcal{R}_g + \mathcal{R}_t + \mathcal{R}_r + \mathcal{R}_s / 3 \end{aligned} \quad (1)$$

where θ_{mod} is a position of the modulator. The total number of flux linkage at the phase U coil is calculated as

$$\begin{aligned} \psi_u &= \left\{ \frac{N^2}{\mathcal{R}_{leak}} + \frac{N^2}{\mathcal{R}_{dc}} + \frac{\mathcal{R}_{mod} N^2}{\mathcal{R}_{dc}^2} \cos(P_{mod} \theta_{mod}) \right\} i_u \\ &\quad - \frac{1}{2} \left\{ \frac{N^2}{\mathcal{R}_{dc}} + \frac{\mathcal{R}_{mod} N^2}{\mathcal{R}_{dc}^2} \cos(P_{mod} \theta_{mod}) \right\} i_v \\ &\quad - \frac{1}{2} \left\{ \frac{N^2}{\mathcal{R}_{dc}} + \frac{\mathcal{R}_{mod} N^2}{\mathcal{R}_{dc}^2} \cos(P_{mod} \theta_{mod}) \right\} i_w \end{aligned} \quad (2)$$

The self-inductance L of each phase and the mutual-inductance M can be derived from (2) as follows:

$$\begin{aligned} L &= \ell + L_{dc} + L_{ac} \cos(P_{mod} \theta_{mod}) \\ M &= -\frac{1}{2} L_{dc} - \frac{1}{2} L_{ac} \cos(P_{mod} \theta_{mod}) \\ \therefore \ell &= \frac{N^2}{\mathcal{R}_{leak}}, L_{dc} = \frac{N^2}{\mathcal{R}_{dc}}, L_{ac} = \frac{\mathcal{R}_{mod} N^2}{\mathcal{R}_{dc}^2} \end{aligned} \quad (3)$$

One of the most significant different features of the MMM from common PM motors is that the number of the stator pole pair is different from that of the rotor. Therefore, the voltage equation of the MMM should be derived by taking the pole pair number difference into account. The magnetomotive force of the rotor PM for each phase \mathcal{F}_u , \mathcal{F}_v , \mathcal{F}_w can be expressed as

$$\begin{aligned} \mathcal{F}_u &= \mathcal{F} \cos(P_{pm} \theta_{pm}) \\ \mathcal{F}_v &= \mathcal{F} \cos\left(P_{pm} \theta_{pm} - \frac{2\pi P_{pm}}{3P_s}\right) \\ \mathcal{F}_w &= \mathcal{F} \cos\left(P_{pm} \theta_{pm} - \frac{4\pi P_{pm}}{3P_s}\right) \end{aligned} \quad (4)$$

where θ_{pm} is a position of the inner PM rotor and \mathcal{F} is the maximum amplitude of the equivalent PM magnetomotive force.

In general, a three-phase voltage equation of the PM motor can be expressed as follows on the stationary reference frame:

$$\begin{bmatrix} v_u \\ v_v \\ v_w \end{bmatrix} = \begin{bmatrix} R & 0 & 0 \\ 0 & R & 0 \\ 0 & 0 & R \end{bmatrix} \begin{bmatrix} i_u \\ i_v \\ i_w \end{bmatrix} + \frac{d}{dt} \begin{bmatrix} L & M & M \\ M & L & M \\ M & M & L \end{bmatrix} \begin{bmatrix} i_u \\ i_v \\ i_w \end{bmatrix} + \frac{d}{dt} \begin{bmatrix} \psi_u \\ \psi_v \\ \psi_w \end{bmatrix}, \quad (5)$$

where R is the stator winding resistance, and ψ_u , ψ_v , and ψ_w are the number of flux linkages for each phase. In the MMM case, it is necessary to consider the number of flux linkage after modulation, which has a relationship such as $\psi_u = L \mathcal{F}_u / N$.

The voltage equation on the $\gamma\delta$ rotating reference frame can be obtained by applying coordinate transformations to (5) as

$$\begin{bmatrix} v_\gamma \\ v_\delta \end{bmatrix} = \begin{bmatrix} R + pL & -\omega L \\ \omega L & R + pL \end{bmatrix} \begin{bmatrix} i_\gamma \\ i_\delta \end{bmatrix} + \begin{bmatrix} -E_\gamma \\ \omega \sqrt{\frac{3}{8}} \frac{L_{ac} \mathcal{F}}{N} - E_\delta \end{bmatrix}. \quad (6)$$

$$\therefore \omega = P_{mod} \omega_{mod} - P_{pm} \omega_{pm}$$

It should be noted that the following rotational angle between the stationary reference frame and the rotating reference frame was used through the rotational coordinate transformation:

$$\theta = \omega t = P_{mod} \omega_{mod} t - P_{pm} \omega_{pm} t = \theta_{mod} - \theta_{pm}, \quad (7)$$

where ω_{pm} and ω_{mod} are mechanical angular frequencies of the inner PM rotor and the modulator, respectively. As is shown in (6), the voltage equation of the MMM is similar to that of the common PM motor whereas some extra electromotive forces are generated by the asynchronous frequency components as follows:

$$\begin{aligned} E_\gamma &= P_{pm} \omega_{pm} \sqrt{\frac{3}{2}} \frac{(\ell + L_{dc}) \mathcal{F}}{N} \sin(P_{mod} \theta_{mod}) \\ &\quad + (P_{mod} \omega_{mod} + P_{pm} \omega_{pm}) \sqrt{\frac{3}{8}} \frac{L_{ac} \mathcal{F}}{N} \sin(2P_{mod} \theta_{mod}) \\ E_\delta &= P_{pm} \omega_{pm} \sqrt{\frac{3}{2}} \frac{(\ell + L_{dc}) \mathcal{F}}{N} \cos(P_{mod} \theta_{mod}) \\ &\quad + (P_{mod} \omega_{mod} + P_{pm} \omega_{pm}) \sqrt{\frac{3}{8}} \frac{L_{ac} \mathcal{F}}{N} \cos(2P_{mod} \theta_{mod}) \end{aligned} \quad (8)$$

The voltage equation has been discussed so far, and a relationship of the electromagnetic torque between the modulator and the inner PM rotor is investigated as follows:

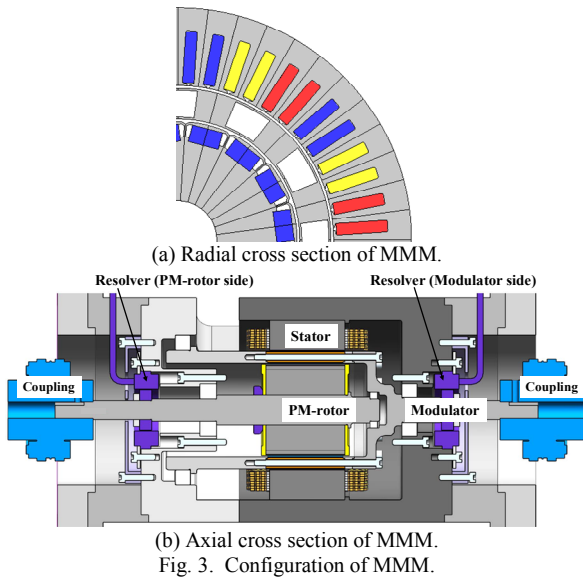
$$\begin{aligned} P_i &= v_\gamma i_\gamma + v_\delta i_\delta = R(i_\gamma^2 + i_\delta^2) + \omega \sqrt{\frac{3}{8}} \frac{L_{ac} \mathcal{F}}{N} i_\delta \\ &= R(i_\gamma^2 + i_\delta^2) + \omega_{mod} \tau_{mod} + \omega_{pm} \tau_{pm} \\ \therefore \tau_{pm} &= -P_{pm} \sqrt{\frac{3}{8}} \frac{L_{ac} \mathcal{F}}{N} i_\delta, \tau_{mod} = P_{mod} \sqrt{\frac{3}{8}} \frac{L_{ac} \mathcal{F}}{N} i_\delta \end{aligned} \quad (9)$$

The above equation is an input electric power, where the first term represents a copper loss of the windings and the second term corresponds to the mechanical output power. Therefore, the following torque relationship can be derived from the result of (9):

$$\tau_s = \frac{P_s}{P_{pm}} \tau_{pm} = -\frac{P_s}{P_{mod}} \tau_{mod}. \quad (10)$$

TABLE I
SPECIFICATIONS OF PROTOTYPE MMM.

Number of stator pole pairs P_s	4
Number of rotor pole pairs P_{pm}	8
Number of modulator cores P_{mod}	12
Stator outer diameter	120 mm
Rotor diameter	61.2 mm
Axial length of core	49.5 mm
Air gap length	0.7 mm
Winding connection	4 series-2 parallel
Maximum current	150 A _{rms}
Armature winding resistance R	33.3 mΩ
Inductance on rotating reference frame L	0.27 mH
Stator flux linkage ψ_a	3.8 mWb



The above equation shows that the MMM works like a planetary gear used as a mechanical power splitter of hybrid vehicles and that the mechanical power can be distributed among the electric power fed by the inverter, mechanical power of the inner PM rotor, and another mechanical power of the modulator.

III. OUTLINE OF PROTOTYPE AND CONFIGURATION OF EXPERIMENTAL SETUP

A small scale prototype of the MMM has been developed to evaluate validity of the proposed vector control technique. TABLE I shows major specifications of a prototype MMM. N39UH (Nd-Fe-B, $B_r = 1.22$ T, $H_{cb} = 965.7$ kA/m@293 K) neodymium PM was employed in the inner rotor. A radial cross section and an axial cross section are shown in Fig. 3, where how the two rotating parts are installed in the prototype is illustrated. In general, the inner PM rotor is mechanically connected to the combustion engine, while the magnetic modulator is connected to the drive shaft in a typical HEV application. The electromagnetic torque is delivered by the MMM according to (10) in either a motoring operation or a regenerating operation.

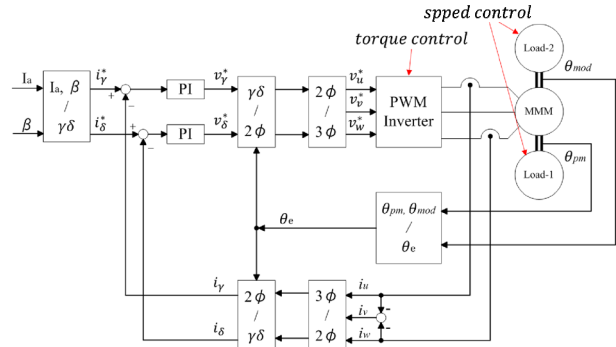


Fig. 4. Block diagram of vector control system for MMM.

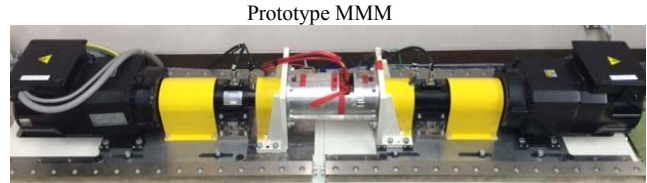


Fig. 5. Experimental setup.

TABLE II
EXPERIMENTAL TEST CONDITIONS.

Inverter DC-bus voltage	80 V
Inverter switching frequency	10 kHz
Dead time	4 μs
Sampling interval of torque	0.5 s

Fig. 4 is a block diagram of the vector control system for the MMM. As can be seen in the figure, two of the resolvers are used to detect the rotational positions of the inner PM rotor and the modulator. The electric angle for rotational coordinate transformation is calculated by (7), and is used for the stator current control which is carried out on the $\gamma\delta$ stator reference frame. For the convenience of the tests, the current commands are given to the controller in a polar coordinate manner, i.e., a current amplitude I_a and a current phase angle β measured from δ -axis.

Fig. 5 shows the experimental setup, where the two load machines are directly connected to the inner PM rotor and the modulator, respectively. The two load machines control their rotation speeds independently. On the other hand, the prototype of the MMM does not have a speed control loop; thus the torque control is only achieved by the controller indicated in Fig. 4. Two of the mechanical output powers from both shafts are measured with two torque meters. The input electric power is also measured with a power meter to evaluate the total power flow. A positive direction for both of the torque and the speed is defined as a CCW rotation of the inner PM rotor.

IV. EXPERIMENTAL TEST RESULTS

A. Experimental Test Conditions

The experimental test conditions are indicated in TABLE II. An inverter was used to operate the prototype MMM, where the DC-bus voltage was 80 V, the switching frequency was 10 kHz, and the dead time was

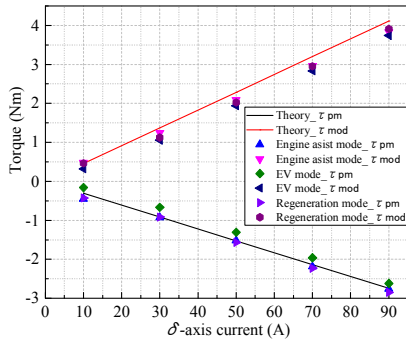


Fig. 6. Output torque and δ -axis current characteristic.

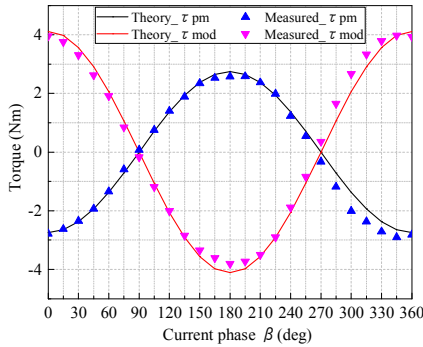


Fig. 7. Output torque and current phase angle β characteristic.

set at $4 \mu s$, respectively. The sampling period of torque measurement was $0.5 s$, and the average torque for $15 s$ was calculated. Many of the compensation control techniques are employed to make the vector control as precise as possible such as a dead time compensation, a discrete time error compensation, an on-voltage compensation of the IGBTs, and so on [7].

B. Output Torque and Equivalent Gear Ratio

A relationship between the torque and the δ -axis current i_δ with the constant $i_\gamma = 0$ is shown in Fig. 6, where i_δ is changed every $20 A$ over the range from 10 to $90 A$. The output torque of the inner PM rotor τ_{pm} and that of the modulator τ_{mod} are delivered in proportional to i_δ regardless of the driving modes. The theoretical relationship between τ_{mod} and τ_{pm} given by (10) is indicated by the solid lines, and the test result agrees with the theoretical relationship of $\tau_{pm} = -2\tau_{mod}/3$.

C. Output Torque and Current Phase Angle

Fig. 7 shows a torque characteristic where the current phase angle β is varied every 15 deg from 0 to 360 deg (electric angle) with constant current vector amplitude of $90 A$ under the engine assist mode. As can be seen in the figure, the torque characteristic similar to an SPMSM is confirmed because of the surface PM structure of the prototype rotor. However, τ_{mod} and τ_{pm} are in opposite phase with each other and their ratio is kept at $\tau_{pm} = -2\tau_{mod}/3$.

D. Confirmation of Voltage Equation

Consistency was examined between the two-axis voltages v_γ and v_δ calculated by (6) and their actual command values in the controller to confirm the validity of the voltage equation. Either i_γ or i_δ was varied in the

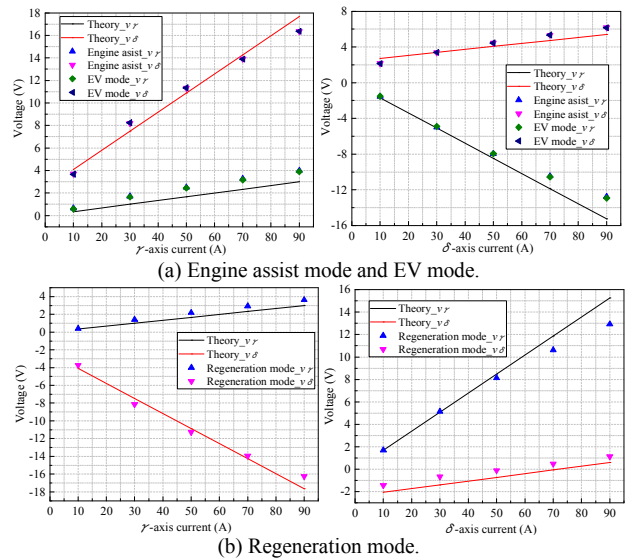


Fig. 8. Confirmation of voltage equation.

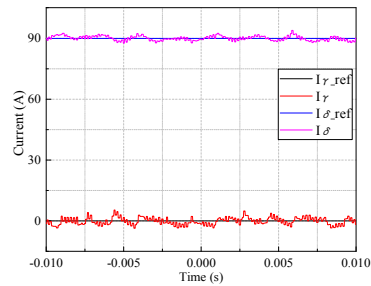
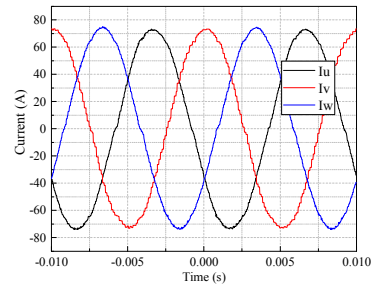


Fig. 9. Current waveforms in EV and regeneration modes.

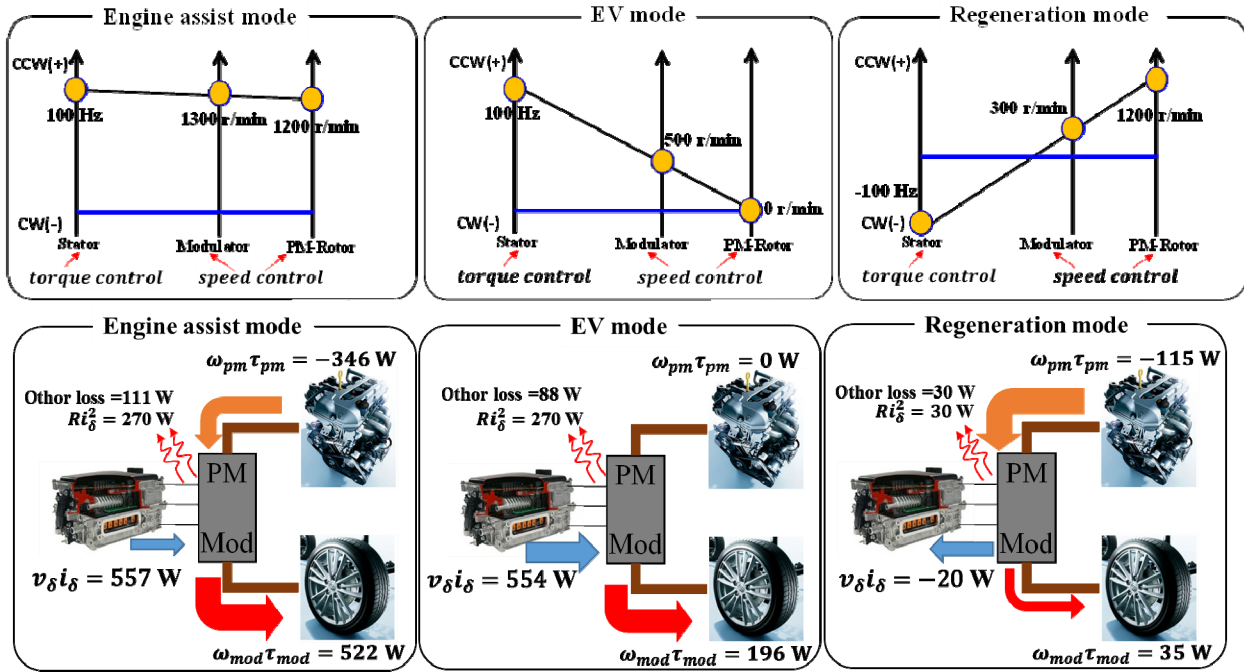


Fig. 10. Three driving modes, collinear charts, and power flow of MMM.

range from 10 to 90 A, and the rest one was kept constant at zero in the tests. The measured and the theoretical results of v_γ and v_δ are shown in Fig. 8, where all the three driving modes are checked. Since the phase sequence and the inverter frequency are identical in the engine assist and the EV modes, both of the characteristics of v_γ and v_δ satisfy the same voltage equation.

$v_\gamma = Ri_\gamma$ and $v_\delta = \omega(Li_\gamma + \psi_a)$ from (6) when $i_\delta = 0$; hence, both of the voltages are proportional to i_γ . In a similar way, if $i_\gamma = 0$ is substituted into (6), $v_\gamma = -\omega Li_\delta$ and $v_\delta = Ri_\delta + \omega\psi_a$ are obtained, which means the voltages are proportional to i_δ . As shown in Fig. 8 (a), actual voltages v_γ and v_δ vary almost linearly, which agrees with their theoretical values indicated by the solid lines. The driving modes, i.e., the engine assist and the EV modes, hardly have influence on the relationships between the voltages and the currents. However, Fig. 8 (a) indicates a slight non linearity due to the magnetic saturation because v_γ or v_δ includes inductance L . Fig. 8 (b) shows v_γ and v_δ in the regenerative operation mode, where either $i_\delta = 0$ or $i_\gamma = 0$ condition is similarly given. The actual values of the voltages agree with their theoretical values for any conditions of the two-axis currents. Therefore, consistency between the mathematical voltage equation of the MMM and the real machine characteristics is appropriately confirmed.

The three-phase currents and the two-axis currents in the EV and the regeneration modes are shown in Fig. 9. The EV mode test condition was $i_\gamma = 0$ and $i_\delta = 90$ A, and the regeneration mode test condition was $i_\gamma = 0$ and $i_\delta = 30$ A. The balanced and sinusoidal three-phase current waveforms are observed in Fig. 9 (a), and the two-axis currents i_γ and i_δ are properly controlled to follow their command values with small deviations. On the other hand, the current waveforms seem to have some ripples

in the regeneration mode shown in Fig. 9 (b), but the vertical axis scale of the graphs is 1/3 of Fig. 9(a). Therefore, the current control in the regeneration mode is properly achieved. As described previously, the regenerating operation makes a phase sequence of the three-phase currents negative.

E. Collinear Chart and Power Flow

Fig. 10 shows collinear charts of the three driving modes that simulate HEV system, i.e., the engine assist mode, the EV mode, and the regeneration mode. The engine assist mode and the EV mode were operated at $i_\gamma = 0$ and $i_\delta = 90$ A, while the regeneration mode was examined at $i_\gamma = 0$ and $i_\delta = 30$ A. The modulator (the drive shaft) speed can be adjustable by changing the inverter frequency and/or the inner PM rotor (the engine) speed in the engine assist mode. On the other hand, the EV mode is achieved by fixing the inner PM rotor (the engine) speed at zero, and the modulator (the drive shaft) speed can be changed by controlling only the inverter frequency. The regeneration mode is achieved by a negative frequency of the inverter.

The test results shown in Fig. 6 indicate that $\tau_{pm} < 0$ and $\tau_{mod} > 0$ when $i_\gamma = 0$ and $i_\delta = 90$ A in the engine assist or the EV mode. The collinear chart depicted in Fig. 10 also indicates that the MMM is operated under the $\omega_{pm} > 0$ and $\omega_{mod} > 0$ condition. Therefore, the mechanical power of the inner PM rotor is negative $\tau_{pm}\omega_{pm} < 0$, i.e., the rotor receives the mechanical power from the load machine (the engine), while the mechanical power of the outer modulator is positive $\tau_{mod}\omega_{mod} > 0$, i.e., the modulator delivers its mechanical power to the load machine (the drive shaft). The supplemental electric power is provided by the inverter, which is converted to the assist mechanical power for the engine in the MMM.

It is found from Fig. 6 that $\omega_{pm} = 0$ and $\omega_{mod} > 0$, and

that $\tau_{mod} > 0$ when $i_\gamma = 0$ and $i_\delta = 90$ A in the EV mode. Therefore, the mechanical power of the inner PM rotor is zero, whereas that of the modulator is positive. This operating condition means that the MMM gives the mechanical power to the load machine through the modulator with standstill inner PM rotor (engine). The inverter provides the MMM with positive electric power in the case; hence, the MMM simply converts the received electric power to the mechanical power.

The surplus mechanical power of the inner PM rotor can be regenerated to the inverter through the stator windings with transferring the requested mechanical power to the modulator (the drive shaft) at the same time. Negative electric power of the inverter $v_\gamma i_\gamma + v_\delta i_\delta < 0$ is a requirement of the regeneration. As described previously in (9), $v_\delta i_\delta < 0$ is the condition of the regeneration mode because of $i_\gamma = 0$. This condition is satisfied in the range of i_δ from 10 to 50 A. In the actual experimental test, the regeneration mode has been achieved when $i_\gamma = 0$ and $i_\delta = 30$ A because the electric power of the inverter is measured negative.

The voltage equation (6) does not include any iron losses and mechanical loss; thus, these losses are residual quantities calculated by the difference between the measured value and the theoretical value. The total of the iron losses and the mechanical loss represented as other losses seems to be more than 15 % of the total input power.

V. CONCLUSIONS

The voltage equation and the torque equation of the magnetically modulated motor have been investigated in the paper. On the basis of the mathematical model, the vector control algorithm has been derived from the voltage equation. In order to confirm the feasibility of the derived vector control algorithm, a prototype was developed and an experimental system was set up. Assuming the three HEV driving modes, i.e., the engine assist, EV, and regeneration modes, various experimental tests were conducted with the prototype motor.

As a result, feasibility of the derived voltage equation was confirmed by comparing the theoretical values calculated from the equation with the measured voltages. The torque equation of the motor is also feasible because it satisfies a relationship of the equivalent gear ratio between the inner PM rotor and the outer magnetic modulator. This characteristic can be represented by collinear charts, which corresponds to a planetary gear actually used as a power splitter of the HEV system.

The power flow of the motor was also investigated through the three driving mode tests. Proper operation was confirmed in every driving mode. However, because the iron loss was dominant in the miniature prototype, high efficiency was not achieved. This iron loss was likely caused by the harmonics of the magnetic flux modulated by the outer modulator, which is a future work to improve the motor efficiency.

REFERENCES

- [1] W. Kaewjinda and M. Konghirun, "A DSP-Based Vector Control of PMSM Servo Drive Using Resolver Sensor," *2006 IEEE Region 10 Conference TENCON*.
- [2] C. C. Mi, G. R. Slemon, and R. Bonert, "Minimization of Iron Losses of Permanent Magnet Synchronous Machines," *IEEE Trans. on Energy Conversion.*, vol. 20, no. 1, pp. 121-127, 2005.
- [3] T. Tonari, H. Kato, and H. Matsui, "Study on Iron Loss of Flux Modulated Type Dual-Axis Motor," *IEEJ RM Tech. Meet.*, RM-13-142, pp. 101-105, 2013.
- [4] M. Fukuoka, K. Nakamura, H. Kato, et al., "A Consideration of the Optimum Configuration of Flux-Modulated Type Dual-Axis Motor," *IEEJ RM Tech. Meet.*, RM-13-141, pp. 95-100, 2013.
- [5] Y. Takeuchi, H. Kato, M. Tago, S. Ogasawara, et al., "Operating Principle and Control Method of the Magnetic Modulated Motor," *IEEJ Conf. Rec.*, no. 5-041, pp. 73-74, 2013.
- [6] M. Aoyama, Y. Kubota, T. Noguchi, et al., "Prototype Design of Permanent-Magnet-Free Magnetic Geared Motor for HEV Application," *IEEJ Ind. Appl. Soc. Conf.*, 3-8, pp. 97-100, 2015.
- [7] J. Kudo, T. Noguchi, M. Kawakami, and K. Sano, "Mathematical Model Errors and Their Compensations of IPM Motor Control System," *IEEJ SPC Tech. Meet.*, SPC-08, pp. 25-30, 2008.